energies

MDPI

Review

A Review of the Visualization Analysis of the Pore-Scale Formation and Decomposition of CO_2 Hydrates for Carbon Capture and Storage

Xuefen Yan [1,2], Jiaxin Liu [1,2], Atsuki Komiya [3], Rachid Bennacer [4] and Lin Chen [1,2,*]

[1] Institute of Engineering Thermophysics, Chinese Academy of Sciences, Beijing 100190, China
[2] University of Chinese Academy of Sciences, Beijing 100049, China
[3] Institute of Fluid Science, Tohoku University, Sendai 980-8577, Japan
[4] LMT-ENS Cachan, CNRS, Paris-Saclay University, 91192 Gif-sur-Yvette, France
* Correspondence: chenlin2018@iet.cn

Abstract

Utilizing microfluidic models, this review synthesizes experimental and simulation insights into the pore-scale behavior of hydrates during formation and decomposition in porous media. It outlines the fundamental characteristics of CO_2 hydrates and their significance in porous media, with a focus on major advancements in hydrate nucleation, growth, distribution, and decomposition kinetics. This study details various porous media systems, visualization experimental setups, and observation techniques employed in experimental research. Key factors, including temperature, pressure, salinity, and pore characteristics, are analyzed to determine their influence on hydrate formation (nucleation, growth kinetics, and phase equilibrium) and decomposition (dissociation kinetics and efficiency) behaviors. In terms of numerical simulation, we distinguishes multiscale numerical simulation methods for the molecular scale, the pore scale, and then the reactor scale, including molecular dynamics simulation, the phase field model, the pore network model, and the macroscopic kinetics model, and discusses the role of simulation in revealing the micro-mechanisms and predicting macroscopic behaviors. This article also summarizes the application of relevant numerical simulation methods (such as MD, CFD, and LBM) in revealing the micro-mechanism of hydrates. Therefore, this review offers critical insights into the micro-mechanisms of carbon dioxide hydrate behavior in porous media, thereby undergirding the theoretical basis for optimizing related engineering designs.

Keywords: flow in porous media; carbon dioxide; hydrate; microfluidic

check for updates

Academic Editor: Alberto Maria Gambelli

Received: 13 November 2025
Revised: 30 November 2025
Accepted: 1 December 2025
Published: 3 December 2025

Citation: Yan, X.; Liu, J.; Komiya, A.; Bennacer, R.; Chen, L. A Review of the Visualization Analysis of the Pore-Scale Formation and Decomposition of CO_2 Hydrates for Carbon Capture and Storage. *Energies* **2025**, *18*, 6344. https://doi.org/10.3390/en18236344

Copyright: © 2025 by the authors. Licensee MDPI, Basel, Switzerland. This article is an open access article distributed under the terms and conditions of the Creative Commons Attribution (CC BY) license (https://creativecommons.org/licenses/by/4.0/).

1. Introduction

In recent decades, hydrate-based technologies have been recognized for their significant and promising application prospects in the energy sector [1,2]. Carbon dioxide hydrates find application in diverse fields such as carbon dioxide sequestration [3–5] and natural gas hydrate exploitation. To advance hydrate technology, a fundamental understanding of their growth behavior and morphological influences is essential. Microfluidic chips are uniquely suited for this purpose, as they offer precise control over temperature, pressure, and flow conditions, enabling the real-time, visual monitoring of hydrate crystal formation.

1.1. Theoretical Aspect of CO_2 Hydrates

In gas hydrates, a cage-like structure with a lattice structure is formed by water molecules through hydrogen bonding, which encloses gaseous molecules (such as CH_4 and CO_2) as ice-like crystalline compounds. Based on variations in hydrogen bond quantity and arrangement, there exist three fundamental crystalline structures: structure I, structure II, and structure H [1,2]. Since the crystal lattice of gas hydrates is composed of water molecules, hydrates have physical properties similar to ice—such as their acoustic characteristics, mechanical properties, and density—except for their thermal conductivity and thermal expansion coefficient, which make commercial-level utilization as an energy resource complicated [1–3,6]. Under high pressure and low temperature, water molecules and carbon dioxide molecules combine to form an ice-like crystalline hydrate—this substance is known as carbon dioxide hydrate.

The processes of gas hydrate formation and decomposition require specific temperature and pressure conditions. The thermodynamics of the hydrate phase equilibrium and reaction kinetics are central to hydrate research. The temperature–pressure conditions corresponding to the complete dissociation endpoint of hydrates are generally regarded as the phase equilibrium conditions. Numerous experiments and simulations have measured phase equilibria for CO_2 hydrates across various systems. The equilibrium conditions and growth morphology of carbon dioxide hydrates have been investigated in four environments: pure water [7–9], different gas compositions [10–12], additives [13–15], and porous media [16–19]. Within a pure water system consisting solely of water molecules and gas molecules, interactions are purely between water and gas molecules, governed solely by temperature and pressure. This system exhibits a well-defined hydrate–liquid water–gas (HLG) phase equilibrium curve. Figure 1 depicts the phase equilibrium diagram for CO_2 hydrate with the temperature ranging from 220 to 300 K and pressure from 0.08 MPa to 8 MPa.

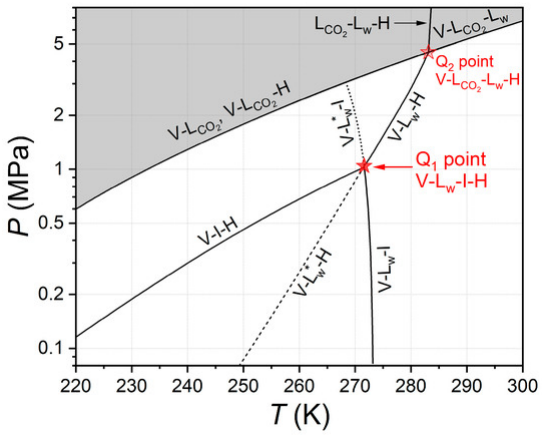


Figure 1. CO_2 hydrate phase equilibrium diagram [9].

Porous media significantly influence the hydrate formation and dissociation mechanisms. Sadeq et al. [16] and Almenningen et al. [17,18] discovered through X-ray micro-CT and NMR imaging that CO_2 hydrates exhibit layered distribution in sandstone, which reduces permeability, while local salinity gradients affect decomposition patterns. Bhattacharjee et al. [19] evaluated the enhanced effects of different porous media like pumice and silica gel on CO_2 hydrate formation kinetics, with pumice achieving a water conversion rate as high as 46%.

The unique characteristic of CO_2 forming into hydrates lies in the fact that under typical hydrate formation temperature and pressure conditions, CO_2 is not in a supercritical state; instead, it can exist in gaseous or liquid form. The various phases of CO_2 determine

its interfacial tension with water and its dissolution rate, and thus affect its mass transfer rate and hydrate formation rate. Under the conditions of pressure exceeding 4.5 MPa and temperature below 283.2 K, CO_2 hydrate forms between water and liquid-phase CO_2. Abe et al. [20] conducted experimental measurements and model estimations of liquid CO_2 hydrate film thickness under varying temperature and flow rate conditions. Li et al. [21] first compared the differences in the formation of gaseous and liquid CO_2 hydrates in micropores, finding that the growth rate of the gas-phase CO_2 hydrate shell is faster, and the coalescence of microbubbles after decomposition is more significant. Furthermore, the state of the water significantly influences this process. At temperatures beneath the water's melting point, ice is thermodynamically stable compared to water. For systems operating at temperatures below water's freezing point, some studies [22–27] have reported and measured equilibrium conditions of the triphasic system involving ice, hydrate, and liquid water. Heidaryan et al. [22] conducted a systematic synthesis of CO_2 hydrate equilibrium data in sub-freezing aqueous systems. Li et al. [23] experimentally investigated the competitive behavior between ice and CO_2 hydrate at temperatures ranging from −10 °C to 0 °C across micron-scale and mesoscale experiments. Their findings revealed that under low subcooling conditions, hydrate formation dominates and replaces ice. Conversely, under high subcooling conditions, ice forms first, followed by the appearance of hydrate as fibrous inclusions surrounding ice crystals. Zhang et al. [26] further noted that ice particle size and temperature significantly impact the hydrate formation kinetics and gas storage performance of CO_2 of sub-freezing point hydrates, with the optimal temperature being 270.15 K. Furthermore, Yang et al. [27] compared conventional formation pathways with freeze–thaw-induced new pathways, finding that ice-mediated nucleation, due to its formation of more porous structures, yields a significant enhancement in hydrate formation rates, with a maximum increase of 48 times.

There are mainly three methods to form hydrates within the system: by fixing one of the three parameters (pressure, temperature, and volume), and altering another to create a thermodynamic driving force for hydrate formation or decomposition [28]. The most common method is the constant volume approach, which maintains the volume of matter within the system unchanged. Hydrates are synthesized in the reaction vessel by lowering the temperature; it is understood that a large number of hydrates are synthesized when the pressure drops sharply. After the synthesis of hydrates is completed, the hydrates are decomposed by slowly increasing the temperature until they are completely decomposed. The intersection of the temperature and pressure curve during decomposition and the temperature and pressure curve before hydrate formation is the equilibrium point of hydrate–liquid water–gas (HLG), that is, the phase equilibrium point of hydrate at this temperature and pressure.

Reaction between water and CO_2 to form a hydrate:

$$CO_2 + nH_2O \rightarrow CO_2 \cdot nH_2O \ \ \Delta H < 0 \quad (1)$$

When the lattice cavity of the structure I hydrate is completely filled with gas, the hydration number n is calculated as 5.75 [26,29]. The maximum gas storage density can then be achieved, capturing 164 m^3 of CO_2 in 1 m^3 of CO_2 hydrate under these conditions [30]. Actually, the hydration number is higher, and the values reported in different studies; CO_2 hydrate exhibits a hydration number spanning 6 to 7 across different temperature conditions [31,32]. Different temperature intervals are usually associated with variations in the formation and dissociation enthalpies of CO_2 hydrates. The properties of hydrates measured under different measurement conditions were summarized [32–35]. The dissociation enthalpy is calculated based on the Clausius–Clapeyron relation via the single-variable slope of the phase equilibrium line [33]. The phase equilibrium pressure of CO_2

hydrate measured by the isochoric process was 1.12 to 3.38 MPa within the temperature interval of 272.65–281.65 K, and calculations utilizing the Clausius–Clapeyron equation gave a dissociation enthalpy of 66.8 kJ/mol.

1.2. Multi-Category Model for Hydrate Formation and Decomposition Processes

Based on a literature survey, several models related to the growth kinetics of gas hydrates are widely recognized. A comprehensive review of methane hydrate growth kinetic models in the public literature was performed by Yin et al. [36].

The formation and decomposition of carbon dioxide hydrate is a complex process involving multiphase and multicomponent transport and reactions. A complete kinetic model typically requires the coupling of multiple sub-models. The following introduces the core equations and models involved in constructing a kinetic model for the formation and decomposition characteristics of CO_2 hydrate.

1.2.1. Fundamental Thermodynamic Models

Before discussing kinetics, it is essential to quantify the reaction driving force—a generic term referring to the thermodynamic imbalance or kinetic gradient that promotes hydrate phase transition (formation or decomposition). Thermodynamic models are employed to calculate the phase equilibrium conditions, thereby identifying the supersaturation or supercooling that acts as the driving force for hydrate phase transitions. Existing computational software can also accurately predict hydrate phase equilibria in the presence of pure water or pure solutions. Currently, the majority of thermodynamic models developed to calculate the phase equilibrium conditions of CO_2 hydrate are derived from modifications to the widely accepted van der Waals–Platteeuw (vDWP) model [37–39].

$$\mu_w^\beta - \mu_w^H = -RT\sum_m \nu_m \ln\left(1 - \sum_j \theta_{mj}\right) \tag{2}$$

where μ_w^β is the water chemical potential in the empty lattice, μ_w^H is the water chemical potential in actual hydrates, v_m is the number of m-type cavities corresponding to each water molecule in the crystal lattice, and θ_{mj} is the occupancy fraction of type m cavities by gas component j.

The core idea of the vDWP model is to regard the cavities in the hydrate lattice as a special adsorption site, where gas molecules are adsorbed. This simplifies the complex hydrate solid problem into a model that can be treated using adsorption isotherm theory. Phase equilibrium is achieved by solving for the chemical potential or fugacity to be equal across all phases [40,41].

1.2.2. Intrinsic Kinetics Model

Intrinsic kinetics describes the chemical reaction rate occurring at the gas–water or hydrate interface, neglecting transfer resistance. The intrinsic reaction rate for hydrate formation is described using Englezos et al.'s model [42]., while the decomposition rate adopts the Kim–Bishnoi model [43]. The core of these two models lies in determining the intrinsic kinetic rate of hydrate reaction and correlating it with the driving force (difference in fugacity) and reaction surface area.

Englezos model [42]:

$$\left(\frac{dn}{dt}\right)_p = K^* A_p (f - f_{eq}) \tag{3}$$

where K^* is defined as the lumped rate parameter (units: mol/m^2·MPa·s), which combines the intrinsic reaction constant and effective mass transfer coefficient, and A_p is the surface area of the single particles.

Due to the difficulty of completely eliminating mass and heat transfer resistances under laboratory conditions, an accurate measurement of the intrinsic formation rate constant has not been achieved, and no universally accepted standard value exists. Consequently, all currently reported CO_2 hydrate formation rate parameters are only apparent K^* values that are strongly dependent on the experimental setup [44–46]. Their calculation is essentially based on the transient gas consumption or mole-number profile, and they must be re-fitted whenever salinity, ion type, or porous-medium characteristics are changed.

Kim–Bishnoi model [43]:

$$-\frac{dn_H}{dt} = k_d \cdot A_s \cdot (f_e - f) \tag{4}$$

where n_H is the total moles of gas encapsulated in the hydrate, A_S is the total surface area of hydrate particles, $f_e - f$ is the fugacity difference (f_e: equilibrium fugacity at equilibrium pressure, f: system fugacity at operating pressure), and k_d is the decomposition rate constant.

The constant k_d is usually written in an Arrhenius-type equation as $k = k_0 \exp(-\Delta E_a/RT)$, in which k_0 is the intrinsic reaction rate constant and ΔEa represents the activation energy. Clarke and Bishnoi [47] measured the intrinsic rate constant of CO_2 hydrate decomposition, k_d = 1.83 × 10^8 mol·m^{-2}·Pa^{-1}·s^{-1} (ΔEa = 102.9 kJ mol^{-1}), in a pure water stirred tank with fully eliminated mass and heat transfer resistance; this was used as an intrinsic benchmark for subsequent studies. Decomposing the intrinsic rate constant has significant limitations: its determination is based on ideal conditions of "no salt, non-porous, and mass and heat transfer without resistance". When salinity or porous media are introduced into the experimental system, corrections need to be made based on the system's characteristics [48,49].

1.2.3. Porous Medium Correction Model

Permeability is a key property of water-bearing porous media, describing the transport capacity of gases and water through the pore structure, directly affecting fluid migration efficiency. However, its application in experimental research [50–52] remains limited due to the technical challenges in monitoring three-phase changes, which are not easily measurable directly. For each phase, the relative permeability needs to be calculated by specific models. These models [53–58] are all based on the renowned Kozeny–Carmon equation in the field of porous media, which has been extensively utilized in studies related to hydrates. The Kozeny–Carmon equation is the most renowned semi-empirical formula in the field of porous media flow, with its core value lying in correlating macroscopic permeability in relation to the medium's microscopic structure, including porosity and specific surface area. It is widely applied in estimating the permeability of porous media.

Kozeny–Carmon equation [55]:

$$k = \frac{1}{C_{K-C}} \frac{\phi^3}{(1-\phi)^2 S_0^2} \tag{5}$$

where k is the permeability of the water-bearing porous media, S_0 is the specific surface area, ϕ is the porosity, and $C_{K\text{-}C}$ is the Kozeny–Carmon constant determined by the type of medium.

2. Mechanism of Hydrate Formation and Dissociation

2.1. Experimental Characterization of Hydrate Formation and Dissociation Processes

2.1.1. Microfluidic Experimental System

Currently, techniques for visualizing the formation and decomposition of gas–water–CO_2 hydrate three-phase interfaces at the microscale of pores remain extremely limited. In recent years, microfluidic visualization technology has demonstrated unique advantages in the study of gaseous hydrates, particularly carbon dioxide hydrates and methane hydrates. This approach not only reveals the mechanisms underlying hydrate formation but also provides theoretical foundations for morphology control and optimization in hydrate storage and transportation technologies.

To conduct the hydrate experiment, the microfluidic visualization experimental device is mainly composed of three parts [59]:

(1) Temperature and pressure control system; This includes the temperature control of the circulating water bath chip and the plunger pump controlling the pressure and injection of the fluid (gas and water).
(2) Visualization systems: Microfluidic visualization chips and holding devices provide a visible pore reaction space, capturing microscopic images of reaction processes and hydrate morphology via microscopes and a high-resolution camera.
(3) Post-processing system: This includes a high-precision temperature and pressure acquisition system and a data imaging processing system.

Figure 2 shows the microfluidic-based experimental setup for investigating the formation and dissociation of pore-scale CO_2 hydrates.

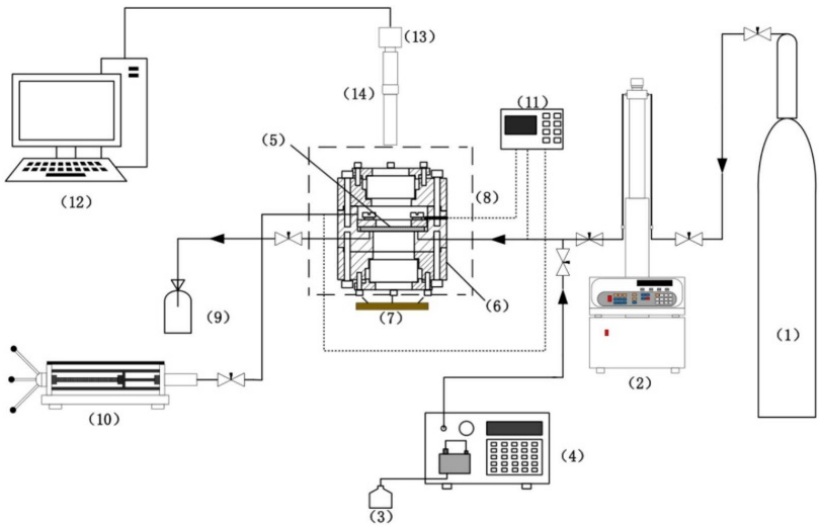


Figure 2. Hydrate formation and dissociation experimental setup diagram [60]. (1) gas/liquid cylinder, (2) gas pump, (3) water container, (4) constant-flow water pump, (5) microfluidic chip, (6) chip holder, (7) optical light source, (8) thermostatic water bath, (9) gas/liquid recovery container, (10) high-pressure pump, (11) T-P acquisition system, (12) real-time data and image acquisition system, (13) camera, (14) microscope.

In the experiment, to form hydrates within the apparatus, a clean, dry microfluidic chip was first installed in the experimental system. The system was evacuated under vacuum, followed by the alternate injection of CO_2 and deionized water into the chip until predetermined pressure and temperature conditions were reached, establishing a stable gas–liquid two-phase environment. Next, through program-controlled manipulation, the system is gradually driven into the hydrate stability zone via gradual cooling or pressure elevation. This induces hydrate crystal nucleation and growth within the

chip, with morphological evolution observed and recorded in real-time via microscopy. Once hydrates are fully formed, hydrate decomposition is triggered by either isothermal depressurization or isobaric heating, while dynamic imaging of decomposition and system pressure/temperature changes is continuously recorded. Upon experiment completion, data acquisition ceases. The system is restored to ambient conditions, cleaned, and prepared for subsequent experiments.

Compared with traditional high-pressure reactors, the unique advantages of this microfluidic system lie in three aspects: (1) Real-time visualization of pore-scale dynamics: It enables the direct observation of hydrate nucleation, growth, and decomposition at the microscale (μm level), which is inaccessible with bulk reactors that only provide macroscopic average data. (2) Precise control of key parameters: Temperature and pressure can be regulated with high accuracy, and fluid flow velocity is adjustable to simulate different reservoir flow conditions. (3) Mimicry of realistic porous media: Microfluidic chips can replicate heterogeneous pore throat structures (e.g., natural sandstone pores or regular geometric models), bridging the gap between idealized laboratory conditions and actual reservoir environments. These advantages make microfluidic technology an indispensable tool for revealing pore-scale hydrate mechanisms.

In microfluidic systems, the quantitative characterization of carbon dioxide hydrate phase transitions relies on a set of key observational parameters. These parameters reveal the thermodynamic and kinetic mechanisms of phase transitions from different dimensions, forming the core indicator system for pore-scale studies. Figure 3 shows the induction time of gas hydrate formation. When the pressure gradually decreases, this indicates that it is in the gas dissolution stage. Since hydrate nucleation is accompanied by rapid gas consumption and instantaneous heat release, it can be identified by an abrupt increase in gas absorption rate and a corresponding sharp exothermic peak in the temperature curve. The induction time [61,62] refers to the interval from the onset of supercooling conditions required for hydrate stability to the first observation of crystal formation. For CO_2 hydrates in porous media, this signifies the onset of nucleation and subsequent formation, which can be determined by identifying the point where local temperature suddenly rises and system pressure decreases significantly. Shortening the induction time is crucial for enhancing CO_2 hydrate formation kinetics, as the induction time also reflects the promotion or inhibition effect on pore-scale hydrate nucleation. Nucleation rate [63,64], defined as the count of newly generated nucleation sites per unit of time and volume, serves as a key parameter for assessing overall nucleation kinetics. Its magnitude directly determines the uniformity of hydrate distribution within porous media. Following the onset of nucleation, hydrate formation proceeds to the growth phase. The growth stage lasts for a duration of time, and when gas absorption ceases, indicating that hydrate growth has reached saturation, it can be concluded that hydrate formation has ended. Since gas consumption [15] is directly proportional to hydrate growth during the growth phase, the hydrate growth rate can be quantified by the slope of the gas absorption curve. Accordingly, the hydrate formation rate is calculated by linearly fitting the gas consumption data against time. The CO_2 hydrate generation rate [65,66] at different temperatures measured in the experiments and the growth activation energy calculated using the Arrhenius equation can be used to characterize CO_2 hydrate kinetics. This parameter reflects the energy barrier that must be overcome during hydrate growth and serves as a key indicator for determining whether the process is diffusion-controlled or interface reaction-controlled.

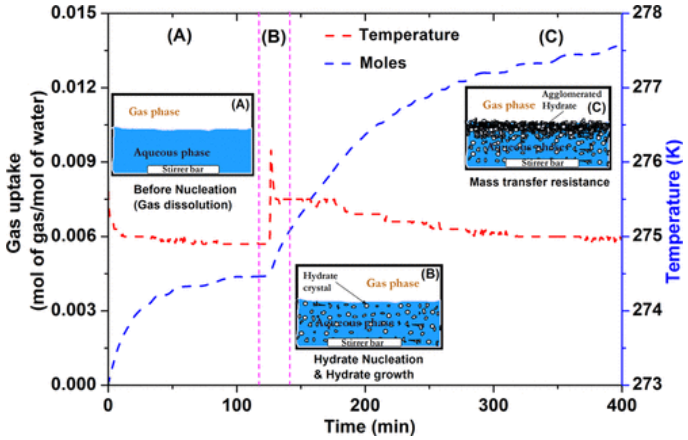


Figure 3. Gas uptake and temperature curves during hydrate formation process [65]. (**A**) Gas dissolution period; (**B**) hydrate nucleation period; (**C**) hydrate growth period. Vertical pink dash lines confines the sudden temperature increase due to dissociation heat release.

The decomposition process of hydrates is central to evaluating the stability of controlled CO_2 release or sequestration. The decomposition temperature/pressure refers to the phase equilibrium point at which the hydrate lattice begins to destabilize and decompose under specific conditions. Decomposition rate [67,68] quantitatively describes the amount of hydrate decomposed per unit time, directly influencing the efficiency of energy extraction or gas release. Closely related to this, the gas productivity [69] directly monitors the dynamic process of CO_2 gas generation during decomposition.

2.1.2. Fluidic Microchannel Chip

The most critical component of the entire experimental apparatus system is the design of the fluidic microchannel chip. When experimental and numerical simulation of the formation and decomposition of CO_2 hydrate in microfluidic systems, the construction of geometric models of porous media is a key first step in determining the realism and complexity of the simulation. In experiments and simulations studying hydrate formation and decomposition, high-pressure resistance and visualization capability are the two core requirements for chip selection.

Researchers typically employ two mainstream strategies.

The first type is an artificial porous medium based on a regular geometric structure, which is a common and effective method in pore-scale simulation. This approach replaces porous media with simple, repetitive geometric units, allowing for the study of fundamental processes in porous media such as multiphase fluid flow and hydrate phase transitions, while ensuring computational feasibility. It is particularly suitable for exploring specific physical mechanisms and validating numerical models. This method includes two main styles. One style employs homogeneous cells to simulate pore structure [21,67,70,71], where solid particles are simplified to regularly arranged spheres, and the gaps between particles form fluid flow channels (Figure 4). Through this method, researchers can precisely control key parameters affecting hydrate nucleation and growth, including porosity and specific surface area, enabling them to study fundamental processes while ensuring computational feasibility. The other style involves designing microchannels with specific geometric structures [72–76]. These designs aim to precisely control fluid dynamics through a combination of experiment and simulation, thereby studying hydrate nucleation and growth. Dehghani et al. [72] developed two novel high-pressure microfluidic systems—a capillary microchannel chip (Figure 5) and a droplet-trapping chip (Figure 6). The capillary channel core allows for the storage of droplets in a single microchannel, while the droplet capture core can more effectively immobilize and control CO_2 droplets or bubbles, preventing their displacement

during the formation of CO_2 hydrates. For pore-scale CO_2 hydrate studies, these specific geometric designs enable high-resolution optical imaging and real-time monitoring of the crystallization process at the CO_2-water interface under static and dynamic flow conditions. By precisely regulating pressure and temperature within the microfluidic chip, the effects of geometric configuration, flow behavior, hydrate morphology evolution, and growth kinetics can be systematically investigated.

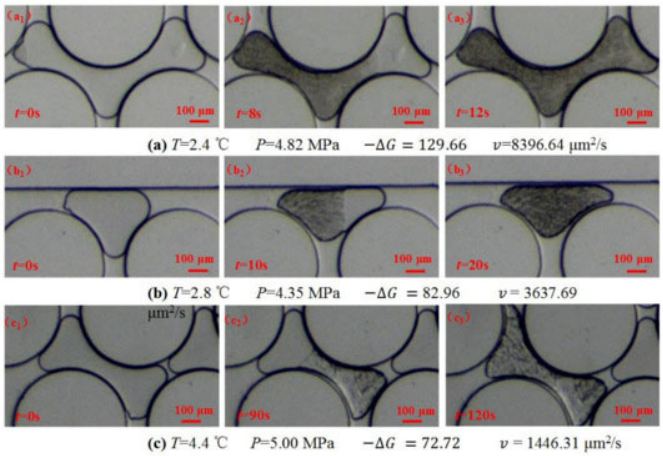


Figure 4. Evolution process of hydrate under different driving forces achieved by homogeneous chip [60]. (**a**) at 2.4 °C and 4.82 MPa. (**b**) at 2.8 °C and 4.35 MPa. (**c**) at 4.4 °C and 5.00 MPa.

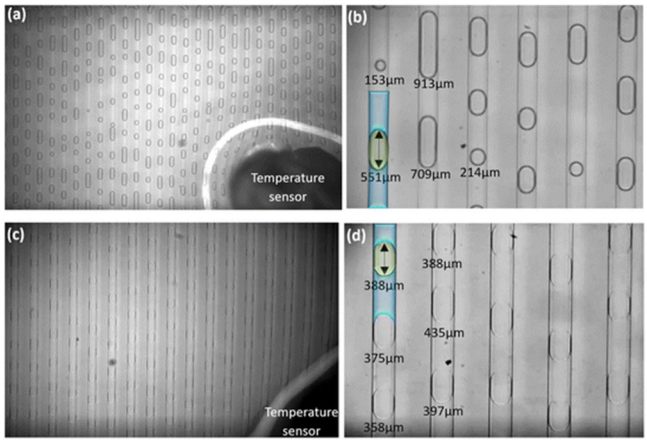


Figure 5. The storage of bubbles achieved by the capillary channel chip [72]; CO_2 is colored green, while water is colored blue. (**a**) overview of bubbles. (**b**) local view. (**c**) regulated bubbles. (**d**) relative smaller sized bubbles.

The second approach involves reconstructing complex porous media based on real rock cores, utilizing micro-CT [77] scan images to construct physical models (Figure 7), and combining them with pore network models for simulation [78,79]. This method can accurately reproduce the heterogeneous microstructure of the medium, including the complex morphology, size distribution, and spatial connectivity of pores and throats, thereby providing a physical field closer to reality for research. This method can accurately reproduce the microstructure of the medium, including the complex morphology, size distribution, and spatial connectivity of pores and throats, thereby providing a physical field closer to reality for research.

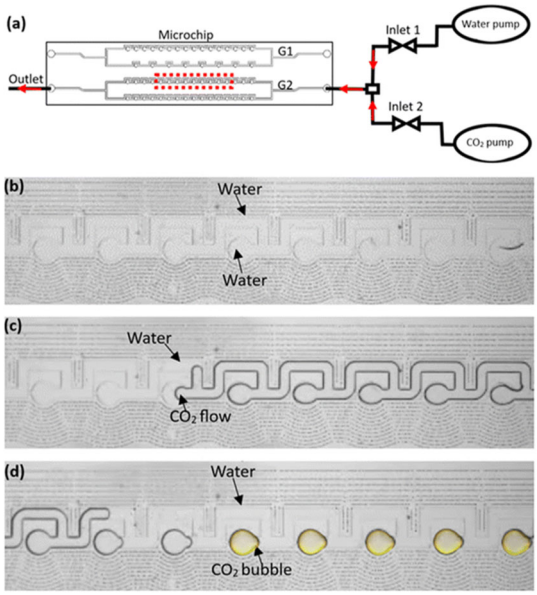


Figure 6. The process of bubble capture achieved by the droplet capture chip [72]. (**a**) Schematic diagram of the device; (**b**) water injection; (**c**) CO_2 injection; (**d**) water injection.

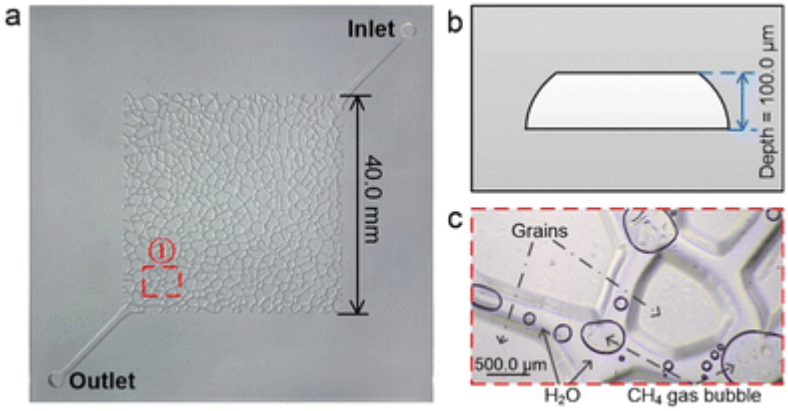


Figure 7. Heterogeneous etching micro-model for CH_4 hydrate formation and dissociation experiments [72] (**a**) Optical photograph of the pore-scale microfluidic chip. (**b**) Schematic cross-sectional profile of the microfluidic chip (**c**) Microscopic image depicting local observation of the pore space (region 1).

The former method focuses on research and parameter analysis, while the latter is used to more realistically reproduce the physical environment within underground reservoirs or experimental chips.

Table 1 lists several typical chip structures, which are the focus of this paper. Combined with microscopic imaging techniques (such as fluorescence microscopy—by adding fluorescent dyes to the aqueous or oil phase, hydrates, water, and gas phases can be clearly distinguished, and the saturation and distribution of each phase can be precisely quantified), this provides a unique perspective for directly observing the phase transition behavior of hydrates at the pore scale, multiphase flow, and their interactions with pore structures.

Table 1. Typical model of porous media chips in microfluidic experiments/simulations.

Reference	Material	Size	Shape	Particle Diameter	Throat Width	Depth	Porosity
Hu et al. (2017) [80]	Silica	2 0 mm × 10 mm	Round grains	590 μm	50 μm	40 μm	0.246
Hou et al. (2018) [81]	Glass	160 × 320, 169 × 338; 200 × 480	Round grains; heterogeneous	40 -	$40\sqrt{2}$ -	-	0.61; 0.53, 0.59
Song et al. (2020) [70]	Glass	16.01 × 16.01 mm; 16.03 × 16.03 mm	Round grains; square grains	250 μm	70 μm	50 μm	0.38; 0.52
Xu et al. (2022) [56]	-	169 × 338 μm; 160 × 320 μm; 169 × $200\sqrt{2}$ μm	Round grains, uniformly arranged in a different array	40 μm 40 μm 45 μm	$40\sqrt{2}$μm	-	0.61; 0.61; 0.5
Ouyang et al. (2025) [82]	Borosilicate	-	Heterogeneous; homogeneous	-	50–700 μm	20 μm	-

2.2. Nucleation Mode and Growth Morphology

CO_2 hydrate formation is a complex, multiphase, and multi-field coupling process, with its core mechanism widely understood as "Dissolution–Nucleation–Growth"—a three-step pathway governing hydrate phase transition. Due to carbon dioxide's high solubility within the aqueous solution, this process initiates with the dissolution of CO_2 molecules at the gas–water interface. Subsequently, these dissolved molecules must diffuse through the interfacial water film near the interface into the bulk aqueous phase. When the CO_2 concentration in the aqueous phase reaches supersaturation, molecules aggregate to form stable nucleation sites, which then grow into hydrate crystals through an ordered crystallization process. Ultimately, the crystals continue growing until they penetrate the water layer and reach the growth front. At the microscopic level, pore-scale studies offer a critical insight into the multiphase flow-coupled understanding of the nucleation and growth mechanisms of hydrates. High-pressure microfluidic visualization, as a powerful experimental tool, enables direct observation of the dynamic competition between homogeneous and heterogeneous nucleation at the pore scale. This technique also allows precise analysis of the complex effects of multiple factors—including temperature, pressure, solution chemistry, and hydrodynamic conditions—on hydrate formation kinetics and bubble evolution patterns [83].

The inherent properties of porous media are key factors determining the formation patterns and distribution of hydrates. Their complex pore structures can severely impede mass transfer, sometimes even causing hydrates to nucleate within the water body or on substrates far from phase boundaries. Wadsworth's research et al. [73] revealed that in confined microenvironments, carbon dioxide hydrates form a unique bilayer structure: one layer consists of a dense, continuous hydrate layer in close contact with liquid water, serving as the primary barrier to mass transfer; the other layer comprises a porous hydrate layer in contact with carbon dioxide gas. The capillary channels within this porous layer provide critical pathways for water and gas transport, serving as a key mechanism enabling the sustained thickening of the hydrate membrane. The heterogeneous distribution of medium partial water saturation and wettability induces spatial variations in hydrate formation, and moderate wettability and partial water saturation conditions may provide the optimal environment for hydrate formation [84]. If the medium is hydrophilic [85] (such as quartz sandstone), water covers the particle surface to form a continuous water film, with CO_2 distributed in the central region of the pores, nucleation occurring at the water–CO_2 interface or in the water, and growing along the water film towards the pore wall to form pore-filling hydrates; if the medium is hydrophobic (some carbonates), CO_2 preferentially contacts the solid surface, with water existing as discrete droplets suspended

in CO_2 and hydrates growing wrapped around the surface of the medium particles to form particle-wrapping hydrates. Li et al. [86] directly observed and verified these two growth patterns under static conditions using a transparent micro-filled bed apparatus. Hauge et al.'s [87] work, which directly observed CO_2 hydrate growth within real pore throat structures using transparent silicon micro-models. This confirmed that hydrate nucleation occurs preferentially at gas–water film interfaces, with secondary nucleation and growth rates significantly outpacing primary nucleation.

The generation process of hydrates also reshapes the flow characteristics within the pores, and the growth pattern and spatial distribution of hydrates determine the macroscopic permeability of porous media. As hydrates grow in the pores, they gradually block the channels of fluid flow, leading to a sharp decrease in the permeability of the medium, thereby inhibiting the supply of reactants (CO_2 and water), causing the growth rate to slow down rapidly. The detection of permeability at the pore scale can reveal this mechanism. Chen et al. [52] conducted experiments in a microchip and directly observed the phase transition process of hydrate formation and decomposition, while analyzing the relationship between hydrate saturation and permeability. Liang et al. [88] assessed how hydrate particle formation and growth patterns affect permeability: they built a 3D cubic pore network model, then used numerical simulations to examine how porous media permeability changes under varying hydrate saturation levels. Their work showed that permeability drops exponentially as hydrate saturation rises.

Innovations in experimental techniques have significantly advanced this field. Within microfluidic experiments, analytical methods such as micro-Raman spectroscopy serve to assess CO_2 hydrate crystallization dynamics. For example, Ouyang et al. [82] combined Raman spectroscopy with microfluidic technology to achieve in situ chemical analysis of the hydrate generation process, revealing the correlation between the different permeability of porous media and nucleation patterns: in low-permeability stochastic and physical pore networks, CO_2 hydrate undergoes homogeneous nucleation (stochastic multi-point nucleation) due to limited CO_2–water mixing; conversely, high-permeability homogeneous pore networks enable non-uniform nucleation (predictable interfacial growth) by promoting continuous gas–liquid interface contact. Wells et al. [89] use Raman technology to quantify the propagation rate of hydrates inside a high-pressure microfluidic device and found that under low supercooling (2 K) and moderate pressure, growth was primarily mass transfer-limited. However, when pressure exceeded a critical threshold, reaction kinetics became the dominant factor restricting growth.

2.3. Decomposition Path and Dynamics

Regarding the decomposition mechanism of carbon dioxide hydrates, there are three mechanisms: thermal stimulation, pressure reduction decomposition, and chemical decomposition. During the decomposition process, hydrates typically begin to decompose from the interface with free fluid (gas or water), forming a clear decomposition front that recedes inward. Research has revealed different patterns of gas migration in the form of discrete bubbles or the formation of continuous flow channels, which are strongly influenced by pore structure, wettability, and decomposition rate. The redistribution of the aqueous phase after decomposition and the process of re-wetting the solid surface also directly affect the subsequent flow path of fluids and mass transfer efficiency. Li et al. [79] revealed distinct dissociation patterns in gas-phase and aqueous-phase hydrates. Dissociation exhibited high synchronization in the gas phase, whereas in the aqueous phase, hydrates in non-gas-invaded fields showed slower dissociation with gradual disintegration. Conversely, hydrates in gas-invaded regions demonstrated significantly accelerated dissociation accompanied by substantial bubble release. Chen et al. [90] innovatively

established a decomposition model that includes heat transfer and intrinsic dynamics, revealing that intrinsic dynamics dominate when the initial hydrate thickness is about 10 μm. Microscopic research intuitively reveals fluid migration phenomena during hydrate formation and microscopic evidence of the "memory effect"—a unique phenomenon where the aqueous phase retains certain structural features after hydrate decomposition. After hydrate decomposition, a certain "structural memory" is retained in part of the aqueous phase, which significantly reduces the nucleation supercooling and accelerates the nucleation rate when hydrates are reformed. Microchip research provides direct evidence for understanding the physical nature of this effect (such as residual nanobubbles, the ordered structure of water molecules). Ji et al. [91] coupled microfluidic platforms with the lattice Boltzmann simulation method to investigate methane hydrate formation and dissociation behaviors in a heterogeneous micro-model, analyzing the permeability evolution of hydrate micro-models during hydrate formation and dissociation. Two hydrate formation mechanisms were observed in porous media: local hydrate decomposition and the hydrate "reformation" phenomenon.

2.4. Factors Affecting Hydrate Behavior

The formation and decomposition of hydrates within porous media constitute a complex dynamic process involving interfacial interactions, mass and heat transfer, and phase transitions among gas, liquid, and solid phases (hydrates and pore walls). The core principle of this process is applied in carbon dioxide hydrate sequestration technology, which involves forming solid hydrates by combining CO_2 with water under specific conditions to stably store CO_2 within underground porous systems encompassing exhausted oil/gas reservoirs and saline aquifers.

The formation kinetics of hydrates strongly depend on external operating conditions. Yu et al. [92] systematically investigated the effects of CO_2 injection rate (6.9–13.8 MPa) and temperature (1.1–9.4 °C) on the formation process. Results indicate that subcooling is the key thermodynamic driver controlling hydrate nucleation rate and ultimate conversion rate. Once the nucleation energy barrier is overcome and stable crystal nuclei form, the system enters the growth phase. Hydrate growth exhibits remarkable morphological diversity, primarily determined by growth conditions such as surface properties, wettability, and degree of undercooling. It can form dense, hard, block-like crystals that severely clog pore spaces, or loose, weakly adherent flocculent or sponge-like structures that have relatively minor impacts on fluid flow. Wang et al. [93] identified five hydrate morphologies—blocky, veiny, spotted, membranous, and shell-like—by introducing methylene blue and confirmed that the existence of free gas increases the decomposition rate by 12 times. The spatial distribution pattern of hydrates is nearly associated with the driving forces within the system. When subcooling or supercritical pressure is low, hydrates tend to grow along pore walls, forming coating structures that uniformly narrow the flow channels. Conversely, under stronger driving forces, hydrates rapidly fill the pores and may even form bridging structures at the throat, leading to severe blockage. Li et al. [60] first quantified the lateral kinetics of CH_4 hydrate films within confined porous media using glass microfluidic chips, revealing that their growth rate positively correlates with the driving force parameter.

The core principle of carbon sequestration technology using carbon dioxide hydrates is to utilize the characteristic of CO_2 and water forming solid hydrates under specific conditions, to fix CO_2 in the form of stable crystals in underground porous media. Wadsworth et al. [73] and Wells et al. [89] studied the phase interface and crystal growth kinetics of CO_2 hydrates using high-pressure silicon-based microfluidic devices, finding that the hydrate conversion rate can reach up to 47% at the microscale, and the reaction time is decreased by 96% in contrast to macroscopic systems. The saline environment reflects the

real geological conditions; the high salinity of underground saline aquifers can change the aggregation state of water molecules, thereby affecting hydrate formation. Salts (such as NaCl) significantly retard the formation of CO_2 hydrates, increase the supercooling required for nucleation, and slow down the growth rate. The visualization results clearly show that the salting-out effect causes hydrates to grow preferentially in specific areas, forming an uneven distribution. Dehghani et al. [94] found that salinity delays nucleation and slows down the growth rate when using cyclopentane hydrates as a substitute for CO_2 hydrates. Kim et al. [95] and Husebø et al. [96] indicate that NaCl concentrations exceeding seawater (3.5 wt%) can lower the phase equilibrium temperature by 2 °C and reduce the hydrate conversion rate to 20–40%. Holzammer et al. [97] quantified that a 20 wt% NaCl solution can reduce the enthalpy of the CO_2 hydrate reaction by 50%. Yanga and Tsai [98] were the first to quantify the volume mass transfer coefficient of supercritical CO_2 in saline water under reservoir conditions (8 MPa, 50 °C), finding that the value is more than 50% higher than that of gaseous/liquid CO_2, and the contribution of the liquid film is dominant. Gautam et al. [99] proposed that hydrophobic amino acids (such as L-leucine) can offset the inhibition by salinity, raising the hydrate conversion rate in freshwater systems to 73%. Ho et al. [100] conducted experimental investigations on the mass transfer rate of CO_2 in aqueous solutions within a microfluidic system under high-pressure conditions, ranging from ground normal state (0.25 MPa, 24 °C) to deep geological reservoir conditions (9.5 MPa, 35 °C). By measuring the changes in length of segmented flows, the liquid-side volumetric mass transfer coefficient was extracted to quantitatively characterize the dynamic mass transfer behavior of bubbles in gaseous, liquid, and supercritical states.

3. Numerical Modeling for Hydrate Research

With the advancement of computational technology, numerical simulation has become an indispensable method in hydrate research. Especially in revealing the fundamental mechanisms of hydrate formation and dissociation, predicting the evolution of reservoir properties, and optimizing exploitation strategies, simulation methods show unique advantages.

When conducting pore-scale numerical simulations of carbon dioxide hydrates within microfluidic systems, the core research focus can be broadly categorized into two main areas: first, concentrating on the microscopic kinetic processes of hydrate formation and decomposition, aiming to reveal their underlying physicochemical mechanisms; second, examining the impact of these processes on the system's overall macroscopic performance (such as permeability, heat and mass transfer efficiency, etc.). These complementary perspectives collectively form a comprehensive understanding of hydrate behavior within porous media.

3.1. Numerical Approaches for Pore-Scale Simulation of CO_2 Hydrate Behavior in Porous Media

Molecular dynamics (MD), computational fluid dynamics (CFD), and the lattice Boltzmann method (LBM) are the main and most widely used numerical approaches for pore-scale numerical simulation of carbon dioxide hydrate in microfluidic systems. Each of them has its own unique theoretical foundation, advantages, and applicable scenarios, and method selection is frequently determined by the specific research requirements, computational resources, and requirements for precision and efficiency.

Molecular dynamics (MD) simulation is a deterministic simulation method founded on Newton's equations of motion. MD excels at uncovering molecular-level mechanisms of hydrate formation and dissociation—such as hydrogen bond network reorganization, guest-molecule encapsulation, and interfacial water structure—yet its nanometer–nanosecond reach precludes direct coupling to flow or field-scale forecasts. In recent years,

researchers [68,85,101–104] have used MD simulation systems to explore the nucleation pathways and stability of hydrates under different conditions. Figure 8 shows the hydrate water system obtained using MD methods. MD simulation is applied to quantify key thermodynamic properties—including diffusion coefficient, thermal conductivity, and heat capacity—of various hydrate structures under specific thermodynamic conditions.

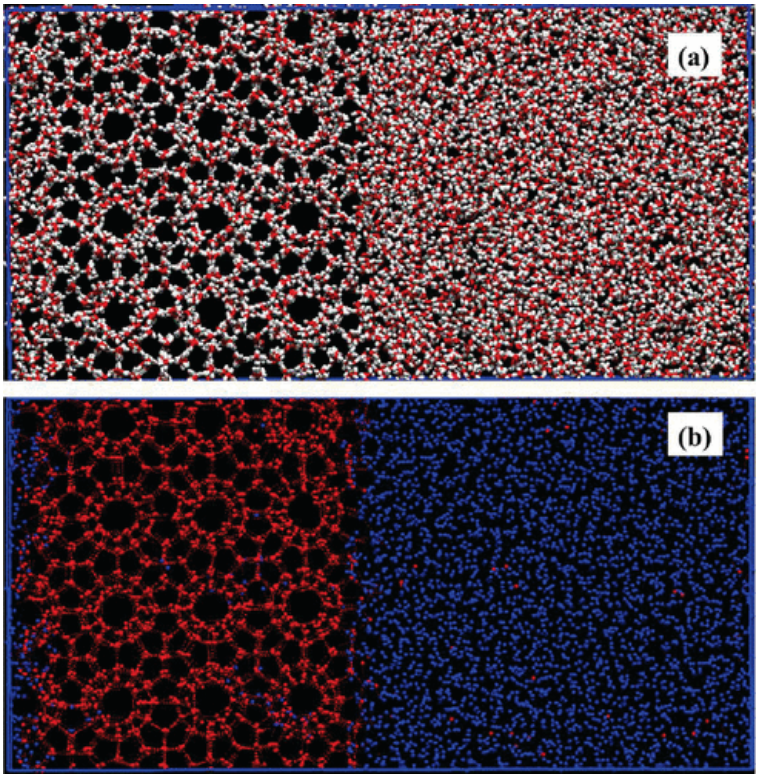


Figure 8. Snapshot of the hydrate−water system obtained using the molecular dynamics method. (**a**) Oxygen and hydrogen atoms are depicted in red and white, respectively. (**b**) Hydrate-like water molecules are highlighted in red and liquid-like water molecules in blue [68].

By solving the Navier–Stokes equation, computational fluid dynamics (CFD) simulations can effectively reproduce the visible flow performance of hydrates in pore networks, including gas–liquid–solid three-phase coupling, interface evolution, and pressure propagation processes. Compared to MD simulations, CFD is suitable for more complex geometries and is particularly suitable for studying the hydrate kinetics of in-pore networks [57,105–109] and their impact on permeability and fluid distribution, but it must rely on empirical constitutive relations for nucleation and other micro-events and carries a heavy grid-generation and interface-tracking burden.

Figure 9 illustrates the modeling of the pore network in hydrates.

In pore-scale simulations, CFD methods are typically combined with interface tracking techniques (such as VOF) to handle multiphase flow and phase transition problems. As the most commonly employed discretization method in CFD, the Finite Volume Method (FVM) has seen extensive application in numerical simulations of fluid flow and heat/mass transfer. It divides the computational domain into a set of non-overlapping control volumes and integrates the governing equations over each control volume to ensure the conservation of physical quantities. When handling multiphase flows, FVM is typically coupled with interface-tracking techniques. Among those, the Volume of Fluid (VOF) method is widely adopted due to its strict conservation properties. VOF tracks the interface between different fluid phases by solving an additional volume fraction transport equation. The VOF method

offers accuracy and credible advantages in tackling intricate multiphase problems and has been validated to be effective in simulating multiphase flow within sophisticated porous media. For instance, in simulating CO_2 hydrate decomposition, the VOF technique can capture the dynamic evolution of the three phase interfaces—CO_2, water, and hydrate—enabling precise calculation of mass and energy exchange during phase transitions.

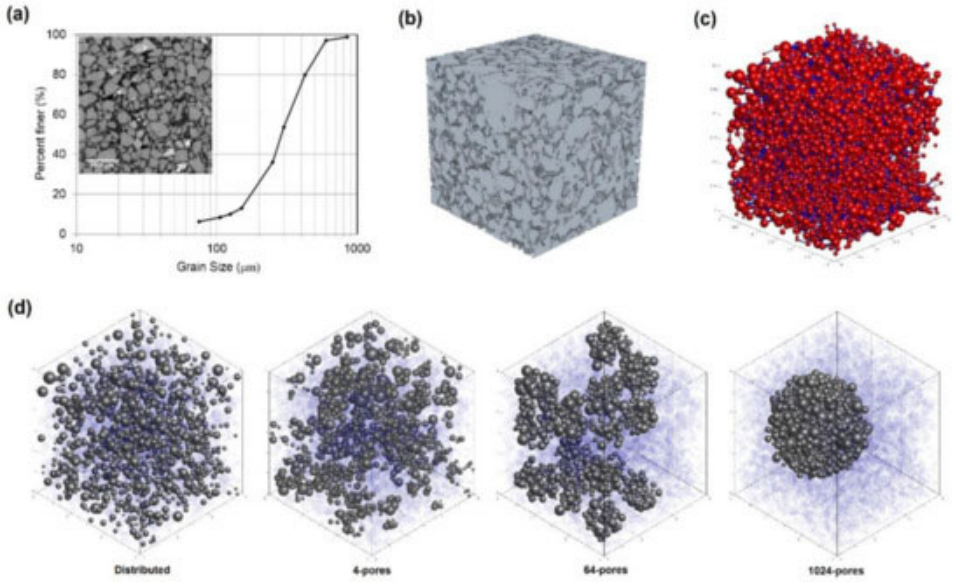


Figure 9. Pore network modeling, constructed by combining micro-CT scanning images. (**a**) Grain size distribution of the specimen. (**b**) The three-dimensional pore space visualized via μCT scanning. (**c**) Pore network model. (**d**) Various hydrate morphologies at a hydrate saturation of Sh = 0.2 [51].

CFD methods demonstrate strong capabilities in modeling heat and mass transfer during hydrate decomposition processes. Jeong et al. [67] used an FVM-based CFD model combined with an unstructured grid to directly numerically simulate the surface decomposition of CO_2 hydrates at the pore scale. Their model takes into account both mass transfer (release of CO_2) and heat transfer to and from water (decomposition endotherms) on the surface of the hydrate.

LBM, rooted in mesoscopic kinetic theory, discretizes fluids into particle distribution functions on lattice points, evolves through collision–migration steps, and then rebounds to obtain macroscopic density and velocity fields. Due to its advantages in complex multiphase flows, it has thus been widely applied in microscopic simulations of hydrate growth and decomposition. Notably, LBM enables spontaneous and heterogeneous hydrate formation within pores while facilitating the calculation of water permeability [110–115]. LBM offers unique advantages over traditional CFD methods in handling complex geometric boundaries and multiphase flows. Since LBM's algorithm is based on grid points, this makes it very convenient to handle complex pore structures directly converted from CT scan images without generating complex computational meshes; its downside is weakened numerical stability under high density/viscosity contrasts or strong non-equilibrium conditions, and its parameters require repeated experimental calibration. LBM is widely used to explore the underlying mechanism by which hydrate formation influences the permeability of porous media. For example, Zhang et al. [113] used LBM to investigate the impact of various factors on hydrate dissociation, and analyzed the relationship between permeability and hydrate saturation. (Figures 10 and 11).

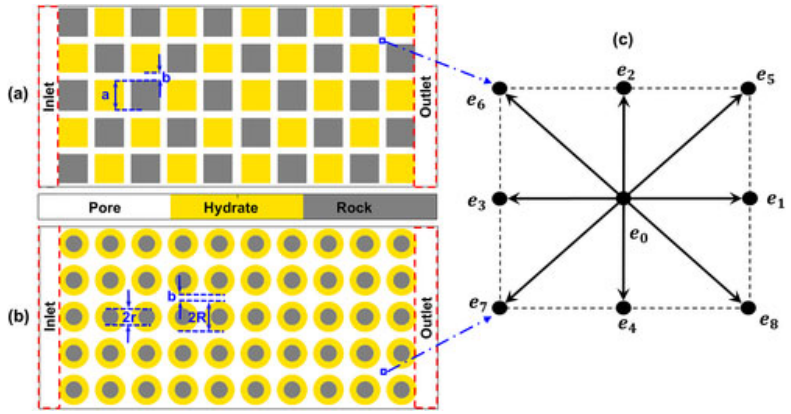


Figure 10. Schematic of porous media and D2Q9 discrete velocity model. (**a**) Pore structure of pore-filling hydrate. (**b**) Pore structure of grain-coating hydrate. (**c**) Schematic of the D2Q9 discrete velocity model [113].

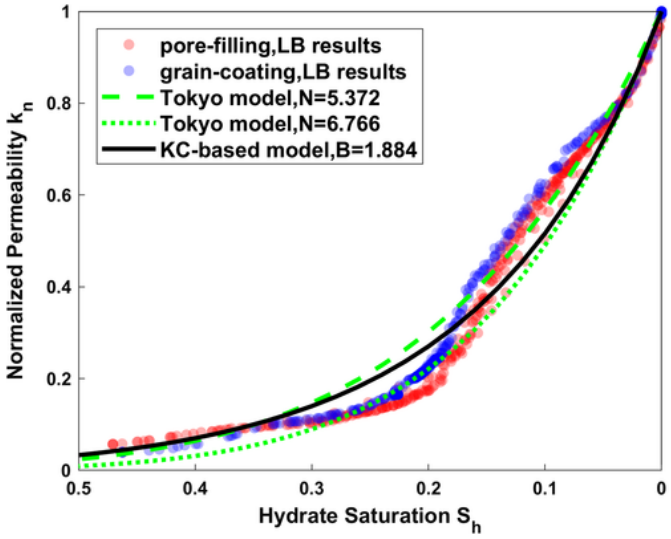


Figure 11. The relationship between permeability and hydrate saturation obtained from the model in Figure 10 using the LBM [113].

3.2. Simulation Results of Formation and Decomposition Kinetics

The experimental results can be combined with numerical simulations to validate and calibrate kinetic models. Zerón et al. [64] investigated the homogeneous nucleation mechanism of CO_2 hydrates within a solution via MD simulations. The study employed the TIP4P/Ice water potential and TraPPE CO_2 force field, analyzing conditions at 400 bar pressure across varying temperatures and CO_2 concentrations. Comparisons with methane hydrates revealed higher nucleation velocities of CO_2 hydrates, which stems from their lower crystal–solution interface free energy. The study further proposes that homogeneous nucleation cannot occur below 20 K under supercooling conditions. Therefore, hydrate formation observed experimentally at low supercooling must result from heterogeneous nucleation. Additionally, the authors specifically verified whether the solution- CO_2 interface influences nucleation, finding that this interface does not affect hydrate nucleation under deep supercooling conditions (40 and 45 K). Algaba et al. [116] focused on the impact of finite-scale effects on the determination of the three-phase coexistence temperature (T_3) of CO_2 hydrates. Employing direct coexistence techniques, the study examined eight pressure conditions and six simulated systems of varying sizes. Findings revealed the emergence of CO_2 droplets in stoichiometric configurations, potentially leading to the overestimation of T_3 values. In contrast, non-stoichiometric large single-cell systems demonstrated T_3 value

convergence, indicating that limited scale effects can be reasonably disregarded when the system scale is sufficiently large. This work underscores the critical importance of initial configuration selection for accurately estimating hydrate triple-point temperatures.

The evolution of phase transition interfaces during hydrate formation and decomposition represents a crucial visualization aspect in pore-scale simulations. Through monitoring the temporal evolution of the gas–liquid–solid three-phase interface, one can gain an intuitive understanding of hydrate growth patterns (such as particle coating, pore filling, bridging, etc.) and their impact on pore space. For instance, in LBM simulations, the evolution of interfaces can be clearly depicted using the Phase Field Method (PFM) or color gradient models [117]. During the CO_2-CH_4 displacement process [118], simulations indicate that initial water tends to be trapped in low-flow pore ends and corner regions, resulting in the formation of pure CO_2 hydrates not only within regions formerly inhabited by CH_4 hydrates but also in zones lacking CH_4 hydrates. Wang et al. [112] established an LBM model coupling salt-dependent hydrate formation kinetics with convection–diffusion equations, discovering that the salt ion repulsion effect reduces guest molecule concentration and slows the hydrate formation rate, though the swift early-stage expansion of hydrate interface area offsets this influence.

The formation and decomposition of hydrates represent sophisticated processes regulated by the synergistic influences of heat and mass transfer, and reaction kinetics. In simulations, the coupling relationships among these three factors must be considered. For instance, during hydrate decomposition, the decomposition reaction absorbs heat (an endothermic reaction). If the heat supply is insufficient, the decomposition rate becomes limited by heat conduction. Simultaneously, CO_2 molecules produced during decomposition must diffuse from the interface into the bulk fluid. If the diffusion rate is slow, a high-concentration boundary layer forms, inhibiting further decomposition. Sean [107] explored the hydrate decomposition kinetic behaviors of CO_2 hydrates within homogeneous porous matrices. Using CFD with unstructured grids, he simulated hydrate decomposition under varying porosity (74%,66%,49%) and temperature–pressure conditions, revealing that reduced porosity inhibits hydrate decomposition. Zhang et al. [113] further developed a coupled non-isothermal multi-physics framework at the pore scale, successfully characterizing the endothermic decomposition behavior of methane hydrates in different assemblage types (pore-filling and particle-encapsulating) and revealing the influence mechanisms of the temperature field, inlet pressure, and inlet temperature conditions on the hydrate decomposition behavior within porous media. Zhang et al. [114] focused on hydrate decomposition, constructing a multiphase, multicomponent LBM model that comprehensively considers decomposition kinetics, gas–water migration, and heat transport. The study revealed that fluid flow significantly accelerates hydrate decomposition, while rapid decomposition within pores may lead to substantial water accumulation and bubble formation.

3.3. Impact on System Characteristics

Accurately characterizing and interpreting the effects of the hydrate reaction process on system properties in numerical simulations is crucial. For instance, in models based on real or regular geometries, wettability is typically characterized by setting the static contact angle between the fluid and solid surfaces. In LBM simulations, different contact angles can be readily achieved by adjusting the interparticle interaction potential [119]. By altering the contact angle value, various wetting conditions can be simulated.

The formation of hydrates occupies pore space, thereby significantly diminishing porous media permeability—a core issue in research. Pore-scale simulations can directly calculate permeability changes before and after hydrate formation, revealing their mi-

croscopic mechanisms. Another study [120] used PFM to construct pore-scale numerical domains encompassing sand grains and coexisting water–CO_2 phases, and investigated how the distribution of micro-hydrates controls effective permeability. Their calculations show that the effective permeability is dependent on the hydrate saturation, the initial aqueous saturation, and the contact angle of water on the surface of sand grains. Lu et al. [121] combined PFM with LBM to model the growth behavior of microscopic CO_2 hydrates in two-phase flow, finding that reduced flow velocity promotes hydrate formation and significantly alters the permeability of the medium. Zhang et al. [57] established a two-dimensional heterogeneous particle size distribution model to investigate how hydrate saturation, distribution patterns, and sediment particle size affect permeability. The study revealed that hydrate distribution patterns (e.g., particle-encapsulating types) could cause a significant permeability drop of up to five orders of magnitude. They established an empirical permeability model that integrates tortuosity and effective porosity. Song et al. [108] investigated the hydrate formation kinetic reaction model, hydrate-induced permeability reduction, and heat/mass transfer models within porous matrices. Using C programming, he developed a subroutine for hydrate formation modeling and solved multiphase flow control equations. The study revealed that both the hydrate reaction surface model and initial fluid distribution significantly influence hydrate formation processes. Notably, even within idealized sealed reactors where water and methane are presumed to mix homogeneously in porous media, the spatial distribution of formed hydrates persists as heterogeneous.

4. Conclusions and Engineering Implications for Carbon Capture and Storage (CCS)

4.1. Engineering Implications for CCS and Future Research Directions

Notably, these pore-scale insights underpin CCS engineering optimization. The pore-filling hydrate growth mode effectively reduces sandstone permeability, demonstrating the potential of CO_2 hydrate as a storage mechanism in the CO_2 storage process [17]. Pore structure evolution regulates CO_2 injection efficiency: expanded pores and enhanced connectivity reduce injection pressure, while excessive hydrate formation or mineral precipitation may cause blockage and fracturing. In long-term storage, hydrate-induced pore filling enhances permanence, while unexpected dissociation threatens reservoir stability. These mechanisms clarify the engineering significance of pore-scale research for CCS.

The relevant achievements deepen understanding of CO_2 hydrate storage and dynamics, providing a robust theoretical foundation and experimental support for advancing carbon dioxide geo-sequestration (CGS) and energy storage technologies.

Despite significant progress, critical gaps remain between the current research and CCS engineering demands. Three targeted future directions are proposed:

First, overcoming the limitations of visualization technologies in 3D dynamic and complex fluid environments. Current studies rely mainly on 2D microfluidic chips [60,78,82] or static 3D characterization [16,17]; future efforts should develop time-lapse micro-CT [51,77], holographic microscopy for real-time 3D tracking, optimize microfluidic chips to simulate complex reservoir fluids [93], and integrate in situ Raman spectroscopy [82,89,90] with 3D visualization to capture morphological and compositional changes simultaneously.

Second, elevating pore-scale mechanisms to macro-reservoir-scale prediction models. Existing simulations excel at pore-scale mechanisms [21,79], but upscaling remains challenging. Future work should establish a multiscale coupling framework (pore network–core–reservoir) [51,88,108], incorporate geological constraints, and validate models with field test data to improve reservoir-scale prediction reliability.

Third, strengthening synergy between experimental visualization and numerical simulation. Current research often separates the two [59,113]; future efforts should use high-precision visualization data to calibrate simulation parameters and leverage simulation results to guide targeted experiments, enhancing mechanism interpretation accuracy and model reliability.

4.2. Conclusions

This review systematically examines the research achievements in the field of microfluidic experiments and multiscale numerical simulations at the pore scale, profoundly elucidating the pore-scale underlying mechanisms of CO_2 hydrate formation and dissociation within reservoir-mimicking porous matrices. The study shows that hydrate behavior is controlled by the "dissolution–nucleation–growth" mechanism, and its nucleation position, growth morphology, and decomposition path are significantly influenced by pore structure, wettability, salinity, and temperature–pressure conditions. At the same time, the hydrate evolution process is accompanied by changes in permeability and fluid redistribution, showing strong dynamic feedback characteristics. The integration of microfluidic visualization technology with simulation methods such as molecular dynamics, CFD, and LBM provides an effective tool for understanding the hydrate–pore coupling mechanism. The relevant achievements not only deepen the understanding of the storage mechanisms and evolutionary dynamics of CO_2 hydrates but also provide a robust theoretical foundation and reliable experimental corroboration for the advancement of geological carbon sequestration (GCS) and energy storage technologies.

Author Contributions: Conceptualization, L.C.; methodology, X.Y. and J.L.; investigation, X.Y. and J.L.; resources, L.C., A.K. and R.B.; data curation, X.Y.; writing—original draft preparation, L.C. and X.Y.; writing—review and editing, L.C., X.Y. and J.L.; supervision, L.C., A.K. and R.B.; project administration, L.C.; funding acquisition, L.C., A.K. and R.B. All authors have read and agreed to the published version of the manuscript.

Funding: This research was funded by the National Natural Science Foundation of China (NSFC), grant number 51961145201; CAS Project for Young Scientists in Basic Research, grant number YSBR043.

Data Availability Statement: The data that support the findings of this study are available within the article.

Conflicts of Interest: The authors declare no conflicts of interest. The funders had no role in the design of the study; in the collection, analyses, or interpretation of data; in the writing of the manuscript, or in the decision to publish the results.

Nomenclature

A_P	Surface area of the particles (m^2)
CH_4	Methane
CO_2	Carbon dioxide
f	Fugacity of the gas (MPa)
f_{eq}	Fugacity of the gas in three-phase equilibrium condition
H	Hydrate
I	Ice
K^*	Combined rate parameter (mol/m^2 MPa s)
k	Permeability of porous media(D)
L_{CO_2}	Liquid carbon dioxide
L_W	Water

L_{W*}	Supercooled water
R	Universal gas constant
S_0	Specific surface area
t	Time (s)
V	Vapor
ϕ	Porosity

References

1. Chen, L.; Merey, S. *Oceanic Methane Hydrates: Fundamentals, Technological Innovations, and Sustainability*; Gulf Professional: Cambridge, MA, USA, 2021.
2. Sloan, E.D. Fundamental Principles and Applications of Natural Gas Hydrates. *Nature* **2003**, *426*, 353–359. [CrossRef] [PubMed]
3. Chen, L.; Sasaki, H.; Watanabe, T.; Okajima, J.; Komiya, A.; Maruyama, S. Production Strategy for Oceanic Methane Hydrate Extraction and Power Generation with Carbon Capture and Storage (CCS). *Energy* **2017**, *126*, 256–272. [CrossRef]
4. Li, M.; Liu, J.; Xia, Y. Risk Prediction of Gas Hydrate Formation in the Wellbore and Subsea Gathering System of Deep-Water Turbidite Reservoirs: Case Analysis from the South China Sea. *Res. Sci.* **2025**, *1*, 52–72. [CrossRef]
5. Wu, J.; Ansari, U. From CO_2 Sequestration to Hydrogen Storage: Further Utilization of Depleted Gas Reservoirs. *Res. Sci.* **2025**, *1*, 19–35. [CrossRef]
6. Ma, Z.W.; Zhang, P.; Bao, H.S.; Deng, S. Review of Fundamental Properties of CO_2 Hydrates and CO_2 Capture and Separation Using Hydration Method. *Renew. Sustain. Energy Rev.* **2016**, *53*, 1273–1302. [CrossRef]
7. Dholabhai, P.D.; Kalogerakis, N.; Bishnoi, P.R. Equilibrium Conditions for Carbon Dioxide Hydrate Formation in Aqueous Electrolyte Solutions. *J. Chem. Eng. Data* **1993**, *38*, 650–654. [CrossRef]
8. Yang, M.; Song, Y.; Liu, Y.; Lam, W.-H.; Li, Q. Equilibrium Conditions for CO_2 Hydrate in Porous Medium. *J. Chem. Thermodyn.* **2011**, *43*, 334–338. [CrossRef]
9. Semenov, A.; Mendgaziev, R.; Stoporev, A.; Istomin, V.; Tulegenov, T.; Yarakhmedov, M.; Novikov, A.; Vinokurov, V. Direct Measurement of the Four-Phase Equilibrium Coexistence Vapor–Aqueous Solution–Ice–Gas Hydrate in Water–Carbon Dioxide System. *Int. J. Mol. Sci.* **2023**, *24*, 9321. [CrossRef] [PubMed]
10. Belandria, V.; Mohammadi, A.H.; Richon, D. Phase Equilibria of Clathrate Hydrates of Methane+Carbon Dioxide: New Experimental Data and Predictions. *Fluid Phase Equilibria* **2010**, *296*, 60–65. [CrossRef]
11. Belandria, V.; Eslamimanesh, A.; Mohammadi, A.H.; Richon, D. Gas Hydrate Formation in Carbon Dioxide + Nitrogen + Water System: Compositional Analysis of Equilibrium Phases. *Ind. Eng. Chem. Res.* **2011**, *50*, 4722–4730. [CrossRef]
12. Belandria, V.; Eslamimanesh, A.; Mohammadi, A.H.; Richon, D. Study of Gas Hydrate Formation in the Carbon Dioxide + Hydrogen + Water Systems: Compositional Analysis of the Gas Phase. *Ind. Eng. Chem. Res.* **2011**, *50*, 6455–6459. [CrossRef]
13. Zhou, X.; Long, Z.; Tang, C.; Liang, D. Kinetic Measurements on CO_2 Hydrate Formation in the Presence of Tetra-n-butyl Ammonium Bromide. *Energy Fuels* **2018**, *32*, 9683–9691. [CrossRef]
14. Jiang, L.; Li, A.; Xu, J.; Liu, Y. Effects of SDS and SDBS on CO_2 Hydrate Formation, Induction Time, Storage Capacity and Stability at 274.15 K and 5.0 MPa. *ChemistrySelect* **2016**, *1*, 6111–6114. [CrossRef]
15. Lee, Y.; Kim, H.; Lee, W.; Kang, D.W.; Lee, J.W.; Ahn, Y.-H. Thermodynamic and Kinetic Properties of CO_2 Hydrates and Their Applications in CO_2 Capture and Separation. *J. Environ. Chem. Eng.* **2023**, *11*, 110933. [CrossRef]
16. Sadeq, D.; Iglauer, S.; Lebedev, M.; Rahman, T.; Zhang, Y.; Barifcani, A. Experimental Pore-Scale Analysis of Carbon Dioxide Hydrate in Sandstone via X-Ray Micro-Computed Tomography. *Int. J. Greenh. Gas Control* **2018**, *79*, 73–82. [CrossRef]
17. Almenningen, S.; Gauteplass, J.; Fotland, P.; Aastveit, G.L.; Barth, T.; Ersland, G. Visualization of Hydrate Formation during CO_2 Storage in Water-Saturated Sandstone. *Int. J. Greenh. Gas Control* **2018**, *79*, 272–278. [CrossRef]
18. Almenningen, S.; Iden, E.; Fernø, M.A.; Ersland, G. Salinity Effects on Pore-Scale Methane Gas Hydrate Dissociation. *J. Geophys. Res. Solid Earth* **2018**, *123*, 5599–5608. [CrossRef]
19. Bhattacharjee, G.; Kumar, A.; Sakpal, T.; Kumar, R. Carbon Dioxide Sequestration: Influence of Porous Media on Hydrate Formation Kinetics. *ACS Sustain. Chem. Eng.* **2015**, *3*, 1205–1214. [CrossRef]
20. Abe, Y.; Ma, X.; Yanai, T.; Yamane, K. Development of Formation and Growth Models of CO_2 Hydrate Film. *AIChE J.* **2016**, *62*, 4078–4089. [CrossRef]
21. Li, X.; Zhao, B.; Wang, C.; Kang, H.; Li, X.; Chen, G.; Sun, C. Investigation on the Gaseous/Liquid CO_2 Hydrate Formation, Growth and Dissociation in Micro-Pores of Microfluidic Chip. *Chem. Eng. Sci.* **2026**, *320*, 122568. [CrossRef]
22. Heidaryan, E.; Robustillo Fuentes, M.D.; Pessôa Filho, P.D.A. Equilibrium of Methane and Carbon Dioxide Hydrates Below the Freezing Point of Water: Literature Review and Modeling. *J. Low Temp. Phys.* **2019**, *194*, 27–45. [CrossRef]
23. Li, Y.; Maria Gambelli, A.; Chen, J.; Yin, Z.; Rossi, F.; Tronconi, E.; Mei, S. Experimental Study on the Competition between Carbon Dioxide Hydrate and Ice below the Freezing Point. *Chem. Eng. Sci.* **2023**, *268*, 118426. [CrossRef]

24. Nagashima, H.D.; Fukushima, N.; Ohmura, R. Phase Equilibrium Condition Measurements in Carbon Dioxide Clathrate Hydrate Forming System from 199.1 K to 247.1 K. *Fluid Phase Equilibria* **2016**, *413*, 53–56. [CrossRef]
25. Melnikov, V.P.; Nesterov, A.N.; Reshetnikov, A.M.; Istomin, V.A.; Kwon, V.G. Stability and Growth of Gas Hydrates below the Ice–Hydrate–Gas Equilibrium Line on the P–T Phase Diagram. *Chem. Eng. Sci.* **2010**, *65*, 906–914. [CrossRef]
26. Zhang, X.; Zhang, M.; Yang, H.; Li, J.; Li, Y.; Wu, Q. Experimental Study on the Formation Characteristics of CO_2 Hydrate in Porous Media below the Freezing Point: Influence of Particle Size and Temperature on the Formation Process and Storage Capacity. *Energy Sci. Eng.* **2022**, *10*, 1164–1176. [CrossRef]
27. Yang, J.; Wang, Y.; Wang, P.; Zhu, J.; Chen, Y.J. Unveiling Gas Hydrate Dynamics: A Microfluidic Investigation of Formation, Decomposition Pathways, and Kinetic Impacts. *Gas Sci. Eng.* **2025**, *142*, 205709. [CrossRef]
28. Semenov, A.P.; Mendgaziev, R.I.; Tulegenov, T.B.; Stoporev, A.S. Analysis of the Techniques for Measuring the Equilibrium Conditions of Gas Hydrates Formation. *Chem. Technol. Fuels Oils* **2022**, *58*, 628–636. [CrossRef]
29. Shindo, Y.; Lund, P.C.; Fujioka, Y.; Komiyama, H. Kinetics and Mechanism of the Formation of CO_2 Hydrate. *Int. J. Chem. Kinet.* **1993**, *25*, 777–782. [CrossRef]
30. Nguyen, N.N.; La, V.T.; Huynh, C.D.; Nguyen, A.V. Technical and Economic Perspectives of Hydrate-Based Carbon Dioxide Capture. *Appl. Energy* **2022**, *307*, 118237. [CrossRef]
31. Velaga, S.C.; Anderson, B.J. Carbon Dioxide Hydrate Phase Equilibrium and Cage Occupancy Calculations Using Ab Initio Intermolecular Potentials. *J. Phys. Chem. B* **2014**, *118*, 577–589. [CrossRef]
32. Voronov, V.P.; Gorodetskii, E.E.; Podnek, V.E.; Grigoriev, B.A. Properties of Equilibrium Carbon Dioxide Hydrate in Porous Medium. *Chem. Phys.* **2016**, *476*, 61–68. [CrossRef]
33. Sloan, E.D. Gas Hydrates: Review of Physical/Chemical Properties. *Energy Fuels* **1998**, *12*, 191–196. [CrossRef]
34. Hu, Q.; Xiao, X. Formation Methods and Applications of Carbon Dioxide Hydrate: An Overview. *Carbon Capture Sci. Technol.* **2023**, *7*, 100113. [CrossRef]
35. Anderson, G.K. Enthalpy of Dissociation and Hydration Number of Carbon Dioxide Hydrate from the Clapeyron Equation. *J. Chem. Thermodyn.* **2003**, *35*, 1171–1183. [CrossRef]
36. Yin, Z.; Khurana, M.; Tan, H.K.; Linga, P. A Review of Gas Hydrate Growth Kinetic Models. *Chem. Eng. J.* **2018**, *342*, 9–29. [CrossRef]
37. Parrish, W.R.; Prausnitz, J.M. Dissociation Pressures of Gas Hydrates Formed by Gas Mixtures. *Ind. Eng. Chem. Process Des. Dev.* **1972**, *11*, 26–35. [CrossRef]
38. Ballard, A.L.; Sloan, E.D., Jr. The next Generation of Hydrate Prediction: I. Hydrate Standard States and Incorporation of Spectroscopy. *Fluid Phase Equilibria* **2002**, *194–197*, 371–383. [CrossRef]
39. Yoon, J.; Chun, M.; Lee, H. Generalized Model for Predicting Phase Behavior of Clathrate Hydrate. *AIChE J.* **2002**, *48*, 1317–1330. [CrossRef]
40. Yang, S.O.; Yang, I.M.; Kim, Y.S.; Lee, C.S. Measurement and Prediction of Phase Equilibria for water+CO_2 in Hydrate Forming Conditions. *Fluid Phase Equilibria* **2000**, *175*, 75–89. [CrossRef]
41. Jäger, A.; Vinš, V.; Gernert, J.; Span, R.; Hrubý, J. Phase Equilibria with Hydrate Formation in H_2O + CO_2 Mixtures Modeled with Reference Equations of State. *Fluid Phase Equilibria* **2013**, *338*, 100–113. [CrossRef]
42. Englezos, P.; Kalogerakis, N.; Dholabhai, P.D.; Bishnoi, P.R. Kinetics of Formation of Methane and Ethane Gas Hydrates. *Chem. Eng. Sci.* **1987**, *42*, 2647–2658. [CrossRef]
43. Kim, H.C.; Bishnoi, P.R.; Heidemann, R.A.; Rizvi, S.S.H. Kinetics of Methane Hydrate Decomposition. *Chem. Eng. Sci.* **1987**, *42*, 1645–1653. [CrossRef]
44. Mekala, P.; Busch, M.; Mech, D.; Patel, R.S.; Sangwai, J.S. Effect of Silica Sand Size on the Formation Kinetics of CO_2 Hydrate in Porous Media in the Presence of Pure Water and Seawater Relevant for CO_2 Sequestration. *J. Pet. Sci. Eng.* **2014**, *122*, 1–9. [CrossRef]
45. Zhang, J.; Lee, J.W. Enhanced Kinetics of CO_2 Hydrate Formation under Static Conditions. *Ind. Eng. Chem. Res.* **2009**, *48*, 5934–5942. [CrossRef]
46. Yang, D.; Le, L.A.; Martinez, R.J.; Currier, R.P.; Spencer, D.F. Kinetics of CO_2 Hydrate Formation in a Continuous Flow Reactor. *Chem. Eng. J.* **2011**, *172*, 144–157. [CrossRef]
47. Clarke, M.A.; Bishnoi, P.R. Determination of the Intrinsic Rate Constant and Activation Energy of CO_2 Gas Hydrate Decomposition Using In-Situ Particle Size Analysis. *Chem. Eng. Sci.* **2004**, *59*, 2983–2993. [CrossRef]
48. Cao, X.; Yang, K.; Xia, W.; Tang, G.; Bian, J. Dissociation Experiment and Dissociation Rate Model of CO_2 Hydrate. *Nat. Gas Ind. B* **2021**, *8*, 607–614. [CrossRef]
49. Rehman, A.N.; Pendyala, R.; Lal, B. Effect of Brine on the Kinetics of Carbon Dioxide Hydrate Formation and Dissociation in Porous Media. *Mater. Today Proc.* **2021**, *47*, 1366–1370. [CrossRef]
50. Seol, Y.; Kneafsey, T.J. Methane Hydrate Induced Permeability Modification for Multiphase Flow in Unsaturated Porous Media. *J. Geophys. Res.* **2011**, *116*, B08102. [CrossRef]

51. Mahabadi, N.; Dai, S.; Seol, Y.; Sup Yun, T.; Jang, J. The Water Retention Curve and Relative Permeability for Gas Production from Hydrate-bearing Sediments: Pore-network Model Simulation. *Geochem. Geophys. Geosyst.* **2016**, *17*, 3099–3110. [CrossRef]
52. Mahabadi, N.; Dai, S.; Seol, Y.; Jang, J. Impact of Hydrate Saturation on Water Permeability in Hydrate-Bearing Sediments. *J. Pet. Sci. Eng.* **2019**, *174*, 696–703. [CrossRef]
53. Fischer, U.; Dury, O.; Flühler, H.; Van Genuchten, M.T. Modeling Nonwetting-Phase Relative Permeability Accounting for a Discontinuous Nonwetting Phase. *Soil Sci. Soc. Am. J.* **1997**, *61*, 1348–1354. [CrossRef]
54. Schäfer, G.; di Chiara Roupert, R.; Alizadeh, A.H.; Piri, M. On the Prediction of Three-Phase Relative Permeabilities Using Two-Phase Constitutive Relationships. *Adv. Water Resour.* **2020**, *145*, 103731. [CrossRef]
55. Zheng, W.; Tannant, D.D. Improved Estimate of the Effective Diameter for Use in the Kozeny–Carman Equation for Permeability Prediction. *Géotech. Lett.* **2017**, *7*, 1–5. [CrossRef]
56. Xu, J.; Bu, Z.; Li, H.; Li, S.; Sun, B. Pore-Scale Flow Simulation on the Permeability in Hydrate-Bearing Sediments. *Fuel* **2022**, *312*, 122681. [CrossRef]
57. Zhang, J.; Liu, X.; Chen, D.; Yin, Z. An Investigation on the Permeability of Hydrate-Bearing Sediments Based on Pore-Scale CFD Simulation. *Int. J. Heat Mass Transf.* **2022**, *192*, 122901. [CrossRef]
58. Kang, D.H.; Yun, T.S.; Kim, K.Y.; Jang, J. Effect of Hydrate Nucleation Mechanisms and Capillarity on Permeability Reduction in Granular Media. *Geophys. Res. Lett.* **2016**, *43*, 9018–9025. [CrossRef]
59. Chen, Y.; Sun, B.; Chen, L.; Wang, X.; Zhao, X.; Gao, Y. Simulation and Observation of Hydrate Phase Transition in Porous Medium via Microfluidic Application. *Ind. Eng. Chem. Res.* **2019**, *58*, 5071–5079. [CrossRef]
60. Li, X.; Wang, C.; Li, Q.; Fan, Q.; Chen, G.; Sun, C. Study on the Growth Kinetics and Morphology of Methane Hydrate Film in a Porous Glass Microfluidic Device. *Energies* **2021**, *14*, 6814. [CrossRef]
61. Golombok, M.; Ineke, E.; Luzardo, J.-C.R.; He, Y.Y.; Zitha, P. Resolving CO_2 and Methane Hydrate Formation Kinetics. *Environ. Chem. Lett.* **2009**, *7*, 325–330. [CrossRef]
62. Yang, M.; Shan, X.; Sun, H.; Chen, B.; Yu, T.; Zhong, D. Review of Thermodynamic and Kinetic Properties of CO_2 Hydrate Phase Transition Process. *Chem. Eng. Sci.* **2025**, *308*, 121383. [CrossRef]
63. Lim, V.W.S.; Barwood, M.T.J.; Metaxas, P.J.; Johns, M.L.; Aman, Z.M.; May, E.F. Nucleation Rates of Carbon Dioxide Hydrate. *Chem. Eng. J.* **2022**, *443*, 136359. [CrossRef]
64. Zerón, I.M.; Algaba, J.; Míguez, J.M.; Grabowska, J.; Blazquez, S.; Sanz, E.; Vega, C.; Blas, F.J. Homogeneous Nucleation Rate of Carbon Dioxide Hydrate Formation under Experimental Condition from Seeding Simulations. *J. Chem. Phys.* **2025**, *162*, 134708. [CrossRef]
65. Kumar, A.; Bhattacharjee, G.; Kulkarni, B.D.; Kumar, R. Role of Surfactants in Promoting Gas Hydrate Formation. *Ind. Eng. Chem. Res.* **2015**, *54*, 12217–12232. [CrossRef]
66. Majid, A.A.A.; Worley, J.; Koh, C.A. Thermodynamic and Kinetic Promoters for Gas Hydrate Technological Applications. *Energy Fuels* **2021**, *35*, 19288–19301. [CrossRef]
67. Jeong, S.-M.; Chiang Hsieh, L.-H.; Huang, C.-Y.; Sean, W.-Y. Direct Numerical Simulation of CO_2 Hydrate Dissociation in Pore-Scale Flow by Applying CFD Method. *Int. J. Heat Mass Transf.* **2017**, *107*, 300–306. [CrossRef]
68. Sarupria, S.; Debenedetti, P.G. Molecular Dynamics Study of Carbon Dioxide Hydrate Dissociation. *J. Phys. Chem. A* **2011**, *115*, 6102–6111. [CrossRef]
69. Sholihah, M.; Sean, W.-Y. Numerical Simulation on the Dissociation, Formation, and Recovery of Gas Hydrates on Microscale Approach. *Molecules* **2021**, *26*, 5021. [CrossRef]
70. Song, Y.; Zhao, C.; Chen, M.; Chi, Y.; Zhang, Y.; Zhao, J. Pore-Scale Visualization Study on CO_2 Displacement of Brine in Micromodels with Circular and Square Cross Sections. *Int. J. Greenh. Gas Control* **2020**, *95*, 102958. [CrossRef]
71. Li, X.; Wang, C.; Li, Q.; Pang, W.; Chen, G.; Sun, C. Experimental Observation of Formation and Dissociation of Methane Hydrate in a Micromodel. *Chem. Eng. Sci.* **2022**, *248*, 117227. [CrossRef]
72. Dehghani, P.; Sinquin, A.; Gland, N.; Lécolier, E.; Ruffine, L.; Tang, A.M. CO_2 Hydrate Nucleation Study: Novel High-Pressure Microfluidic Devices. *Lab Chip* **2025**, *25*, 2903–2917. [CrossRef] [PubMed]
73. Wadsworth, L.A.; Balke, J.G.; Hartman, R.L.; Koh, C.A. Carbon Dioxide Hydrate Crystallization Thickening & Morphology in a Micro-Confined Environment for Carbon Capture & Sequestration Processes. *Appl. Energy* **2024**, *371*, 123664. [CrossRef]
74. Martinez de Baños, M.L.; Carrier, O.; Bouriat, P.; Broseta, D. Droplet-Based Millifluidics as a New Tool to Investigate Hydrate Crystallization: Insights into the Memory Effect. *Chem. Eng. Sci.* **2015**, *123*, 564–572. [CrossRef]
75. Marre, S.; Adamo, A.; Basak, S.; Aymonier, C.; Jensen, K.F. Design and Packaging of Microreactors for High Pressure and High Temperature Applications. *Ind. Eng. Chem. Res.* **2010**, *49*, 11310–11320. [CrossRef]
76. Sun, Q.; Du, M.; Li, X.; Guo, X.; Yang, L. Morphology Investigation on Cyclopentane Hydrate Formation/Dissociation in a Sub-Millimeter-Sized Capillary. *Crystals* **2019**, *9*, 307. [CrossRef]
77. Lv, J.; Zhao, J.; Jiang, L.; Liu, Y.; Mu, H. A Review of Micro Computed Tomography Studies on the Gas Hydrate Pore Habits and Seepage Properties in Hydrate Bearing Sediments. *J. Nat. Gas Sci. Eng.* **2020**, *83*, 103555. [CrossRef]

78. Xu, R.; Kou, X.; Wu, T.-W.; Li, X.-S.; Wang, Y. Pore-Scale Experimental Investigation of the Fluid Flow Effects on Methane Hydrate Formation. *Energy* **2023**, *271*, 126967. [CrossRef]
79. Li, Y.; Xie, Y.; Zhang, K.; Wu, P.; Song, Y. CO_2 Hydrate Microscopic Phase Transition Behavior Based on Microfluidic Chips. *Energy* **2025**, *338*, 138944. [CrossRef]
80. Hu, R.; Wan, J.; Kim, Y.; Tokunaga, T.K. Wettability Effects on Supercritical CO_2–Brine Immiscible Displacement during Drainage: Pore-Scale Observation and 3D Simulation. *Int. J. Greenh. Gas Control* **2017**, *60*, 129–139. [CrossRef]
81. Hou, J.; Ji, Y.; Zhou, K.; Liu, Y.; Wei, B. Effect of Hydrate on Permeability in Porous Media: Pore-Scale Micro-Simulation. *Int. J. Heat Mass Transf.* **2018**, *126*, 416–424. [CrossRef]
82. Ouyang, Q.; Komisar, D.; Ilchenko, O.; von Solms, N.; Pandey, J.S. Raman Assisted Microfluidic Insights into CO_2 Hydrate Dynamics and Subsurface Sequestration in Confined Space. *Chem. Eng. J.* **2025**, *513*, 162897. [CrossRef]
83. Zhang, J.; Yin, Z.; Li, Q.; Li, S.; Jiao, H.; Liu, X. An investigation on CH_4 hydrate transition and gas bubble evolution on microfluidic chip. *Chin. J. Theor. Appl. Mech.* **2024**, *56*, 1615–1623.
84. Nguyen, N.N.; Galib, M.; Nguyen, A.V. Critical Review on Gas Hydrate Formation at Solid Surfaces and in Confined Spaces—Why and How Does Interfacial Regime Matter? *Energy Fuels* **2020**, *34*, 6751–6760. [CrossRef]
85. Bai, D.; Chen, G.; Zhang, X.; Wang, W. Microsecond Molecular Dynamics Simulations of the Kinetic Pathways of Gas Hydrate Formation from Solid Surfaces. *Langmuir* **2011**, *27*, 5961–5967. [CrossRef]
86. Li, X.; Liu, M.; Li, Q.; Pang, W.; Chen, G.; Sun, C. TBAB Hydrate Formation and Growth in a Microdevice under Static and Dynamic Conditions. *Pet. Sci.* **2024**, *21*, 1396–1404. [CrossRef]
87. Hauge, L.P.; Gauteplass, J.; Høyland, M.D.; Ersland, G.; Kovscek, A.; Fernø, M.A. Pore-Level Hydrate Formation Mechanisms Using Realistic Rock Structures in High-Pressure Silicon Micromodels. *Int. J. Greenh. Gas Control* **2016**, *53*, 178–186. [CrossRef]
88. Liang, H.; Song, Y.; Liu, Y.; Yang, M.; Huang, X. Study of the Permeability Characteristics of Porous Media with Methane Hydrate by Pore Network Model. *J. Nat. Gas Chem.* **2010**, *19*, 255–260. [CrossRef]
89. Wells, J.D.; Chen, W.; Hartman, R.L.; Koh, C.A. Carbon Dioxide Hydrate in a Microfluidic Device: Phase Boundary and Crystallization Kinetics Measurements with Micro-Raman Spectroscopy. *J. Chem. Phys.* **2021**, *154*, 114710. [CrossRef] [PubMed]
90. Chen, W.; Hartman, R.L. Methane Hydrate Intrinsic Dissociation Kinetics Measured in a Microfluidic System by Means of in Situ Raman Spectroscopy. *Energy Fuels* **2018**, *32*, 11761–11771. [CrossRef]
91. Ji, Y.; Hou, J.; Zhao, E.; Liu, C.; Guo, T.; Liu, Y.; Wei, B.; Bai, Y. Pore-Scale Study on Methane Hydrate Formation and Dissociation in a Heterogeneous Micromodel. *J. Nat. Gas Sci. Eng.* **2021**, *95*, 104230. [CrossRef]
92. Yu, W.; Habiburrahman, M.; Sultan, A.S. Microfluidic Study of Hydrate Propagation during CO_2 Injection into Cold Aquifers. *Carbon Capture Sci. Technol.* **2025**, *15*, 100401. [CrossRef]
93. Wang, Y.; Yang, J.; Wang, P.; Zhu, J.; Chen, Y.J. Impact of Multiphasic Pore-Scale Interactions on Gas Hydrate Formation and Dissociation Characteristics and Kinetics: A Microfluidic Study. *Lab Chip* **2025**, *25*, 3741–3765. [CrossRef] [PubMed]
94. Dehghani, P.; Sinquin, A.; Gland, N.; Tang, A.M.; Estublier, A. Investigating Cyclopentane Hydrate Nucleation and Growth Using Microfluidics. *Sci. Technol. Energy Transit.* **2023**, *78*, 36. [CrossRef]
95. Kim, S.; Park, M.; Mok, J.; Seo, Y. Salinity-Controlled Guest Selectivity in CH_4 + CO_2 Hydrates: Implications for Enhanced CO_2 Sequestration in Marine Sediments. *J. Environ. Chem. Eng.* **2025**, *13*, 119500. [CrossRef]
96. Husebø, J.; Ersland, G.; Graue, A.; Kvamme, B. Effects of Salinity on Hydrate Stability and Implications for Storage of CO_2 in Natural Gas Hydrate Reservoirs. *Energy Procedia* **2009**, *1*, 3731–3738. [CrossRef]
97. Holzammer, C.; Finckenstein, A.; Will, S.; Braeuer, A.S. How Sodium Chloride Salt Inhibits the Formation of CO_2 Gas Hydrates. *J. Phys. Chem. B* **2016**, *120*, 2452–2459. [CrossRef] [PubMed]
98. Yang, J.; Tsai, P.A. Microfluidic Mass Transfer of Supercritical CO_2 in Brine. *Chem. Eng. Sci.* **2024**, *300*, 120543. [CrossRef]
99. Gautam, R.; Kumar, S.; Kumar, A. Intensified Carbon Dioxide Hydrate Formation Kinetics in a Simulated Subsea Sediment: Application in Carbon Capture and Sequestration. *Energy Fuels* **2022**, *36*, 9194–9202. [CrossRef]
100. Ho, T.-H.M.; Yang, J.; Tsai, P.A. Microfluidic Mass Transfer of CO_2 at Elevated Pressures: Implications for Carbon Storage in Deep Saline Aquifers. *Lab Chip* **2021**, *21*, 3942–3951. [CrossRef]
101. Palodkar, A.V.; Dongre, H.J.; Thakre, N.; Jana, A.K. Microsecond Molecular Dynamics of Methane–Carbon Dioxide Swapping in Pure and Saline Water Environment. *Sci. Rep.* **2022**, *12*, 2634. [CrossRef]
102. Yu, Q.; Li, C.; Peng, B.; Tang, H.; Yang, T.; Yu, Y.; Zhang, K.; Chen, Z. Research Progress and Outlook of Molecular Dynamics Simulation on Carbon Dioxide Applied for Methane Exploitation from Hydrates. *Molecules* **2024**, *29*, 5579. [CrossRef] [PubMed]
103. Hao, X.; Li, C.; Meng, Q.; Sun, J.; Huang, L.; Bu, Q.; Li, C. Molecular Dynamics Simulation of the Three-Phase Equilibrium Line of CO_2 Hydrate with OPC Water Model. *ACS Omega* **2023**, *8*, 39847–39854. [CrossRef]
104. Uddin, M.; Coombe, D. Kinetics of CH_4 and CO_2 Hydrate Dissociation and Gas Bubble Evolution via MD Simulation. *J. Phys. Chem. A* **2014**, *118*, 1971–1988. [CrossRef]
105. Li, G.; Zhan, L.; Yun, T.; Dai, S. Pore-Scale Controls on the Gas and Water Transport in Hydrate-Bearing Sediments. *Geophys. Res. Lett.* **2020**, *47*, e2020GL086990. [CrossRef]

106. Li, Z.; You, J.; Qin, G. Pore-Scale Modellings on the Impacts of Hydrate Distribution Morphology on Gas and Water Transport in Hydrate-Bearing Sediments. In Proceedings of the SPE Canadian Energy Technology Conference, Calgary, AB, Canada, 11 March 2022; p. D022S010R002.
107. Sean, W.-Y. Direct Numerical Simulation of Hydrate Dissociation in Homogeneous Porous Media by Applying CFD Method: One Example of CO_2 Hydrate. In *Heat and Mass Transfer—Advances in Modelling and Experimental Study for Industrial Applications*; IntechOpen: London, UK, 2018; ISBN 978-1-78923-773-3.
108. Song, R.; Sun, S.; Liu, J.; Feng, X. Numerical Modeling on Hydrate Formation and Evaluating the Influencing Factors of Its Heterogeneity in Core-Scale Sandy Sediment. *J. Nat. Gas Sci. Eng.* **2021**, *90*, 103945. [CrossRef]
109. Yu, P.-Y.; Sean, W.-Y.; Yeh, R.-Y.; Chiang Hsieh, L.-H.; Hsu, R.-Q.; Sato, T. Direct Numerical Simulation of Methane Hydrate Dissociation in Pore-Scale Flow by Using CFD Method. *Int. J. Heat Mass Transf.* **2017**, *113*, 176–183. [CrossRef]
110. Jiang, F.; Hu, C. *Application of Lattice Boltzmann Method for Simulation of Turbulent Diffusion from a CO_2 Lake in Deep Ocean*; Kyushu University: Fukuoka, Japan, 2012.
111. Succi, S.; Moradi, N.; Greiner, A.; Melchionna, S. Lattice Boltzmann Modeling of Water-like Fluids. *Front. Phys.* **2014**, *2*, 22. [CrossRef]
112. Wang, Q.; Han, D.; Wang, Z.; Ma, Q.; Wang, D. Lattice Boltzmann Modeling for Hydrate Formation in Brine. *Chem. Eng. J.* **2019**, *366*, 133–140. [CrossRef]
113. Zhang, L.; Zhang, C.; Zhang, K.; Zhang, L.; Yao, J.; Sun, H.; Yang, Y. Pore-Scale Investigation of Methane Hydrate Dissociation Using the Lattice Boltzmann Method. *Water Resour. Res.* **2019**, *55*, 8422–8444. [CrossRef]
114. Zhang, Y.; Wang, X.; Dong, B.; An, X.; Chen, C.; Zhou, X.; Li, W. Numerical Simulation of Methane Hydrate Dissociation Characteristics in Microporous Media Using Lattice Boltzmann Method: Effect of Fluid Flow. *Chem. Eng. Sci.* **2023**, *267*, 118384. [CrossRef]
115. Hao, L.; Cheng, P. Pore-Scale Simulations on Relative Permeabilities of Porous Media by Lattice Boltzmann Method. *Int. J. Heat Mass Transf.* **2010**, *53*, 1908–1913. [CrossRef]
116. Algaba, J.; Blazquez, S.; Feria, E.; Míguez, J.M.; Conde, M.M.; Blas, F.J. Three-Phase Equilibria of Hydrates from Computer Simulation. II. Finite-Size Effects in the Carbon Dioxide Hydrate. *J. Chem. Phys.* **2024**, *160*, 164722. [CrossRef]
117. Yamaguchi, A.J.; Sato, T.; Nono, A.; Tobase, T. Numerical Simulation of Permeability Change in Porous Media by the Formation of CO_2 Hydrate. In Proceedings of the OCEANS 2022, Chennai, India, 21–24 February 2022.
118. Wang, Y.; Wu, X.; Zhang, Y.; Yin, C.; Dong, B.; Li, W. Impact of Pore Structure and Hydrate Distribution on CO_2-CH_4 Replacement in CH_4 Hydrate: A Pore-Scale Numerical Analysis. *Energies* **2025**, *18*, 2519. [CrossRef]
119. Liu, Q.; Li, J.; Liang, B.; Sun, W.; Liu, J.; Lei, Y. Microscopic Flow of CO_2 in Complex Pore Structures: A Recent 10-Year Review. *Sustainability* **2023**, *15*, 12959. [CrossRef]
120. Fuji, T.; Kamada, K.; Sato, T.; Oyama, H.; Yamaguchi, A.J.; Tobase, T. Numerical Simulation of Crystal Growth of CO_2 Hydrate within Microscopic Sand Pores Using Phase Field Model for the Estimation of Effective Permeability. *Int. J. Greenh. Gas Control* **2020**, *95*, 102960. [CrossRef]
121. Lu, S.; Yamaguchi, A.J.; Kobayasi, K.; Sato, T.; Tobase, T. Numerical Simulation of Microscopic Carbon Dioxide Hydrate Formation in Two-Phase Flow. In Proceedings of the OCEANS 2022, Chennai, India, 21–24 February 2022; pp. 1–6.

Disclaimer/Publisher's Note: The statements, opinions and data contained in all publications are solely those of the individual author(s) and contributor(s) and not of MDPI and/or the editor(s). MDPI and/or the editor(s) disclaim responsibility for any injury to people or property resulting from any ideas, methods, instructions or products referred to in the content.